

Research Article

Variability of Bimodal Soil-Water Characteristic Curves under Different Confining Pressures

Achmad Syarifudin  and Alfredo Satyanaga 

Civil and Environmental Engineering Faculty, Universitas Bina Darma, Palembang 30264, Indonesia

Correspondence should be addressed to Alfredo Satyanaga; alfrendonio@yahoo.com.sg

Received 3 February 2021; Accepted 23 May 2021; Published 7 June 2021

Academic Editor: Maman Turjaman

Copyright © 2021 Achmad Syarifudin and Alfredo Satyanaga. This is an open access article distributed under the Creative Commons Attribution License, which permits unrestricted use, distribution, and reproduction in any medium, provided the original work is properly cited.

Soils with two subcurves of Soil-Water Characteristic Curve (SWCC) (dual porosity soils) might be found within various residual soils. Soils located in different depths have different confining pressure. Residual soils are found in the unsaturated zones due to the deep groundwater table. There is a linear correlation between the hydraulic properties of the soil in the unsaturated area and that of its unsaturated properties. This study aims to examine the influence of the confining pressure towards the SWCC of dual porosity soil. The scope of this study involves measurements of the drying and wetting SWCC using Tempe cells, pressure plates, and an advanced triaxial apparatus. In this study, the mathematical equations were developed to explain the effect of confining pressure on SWCC. The experimental results indicated that the dual porosity soil exhibits bimodal characteristics for the drying curve of SWCC and it exhibits unimodal characteristics for the wetting curve of SWCC. As the confining pressure increases, the air entry values, the inflection points, and the standard deviation of drying SWCC increase. In addition, the hysteresis of SWCC is becoming smaller with the increasing confining pressure.

1. Introduction

Saturated soil consists solely of soil solids and water as the air spaces within have been filled with water. The principles of classical soil mechanics can be used to correlate the properties and behavior of saturated soil. Unsaturated soil has voids within that contain water partially comprising soil entities, water, and a combination of water and air in its fourth phase termed contractile skin [1, 2]. As a result of the various phases, the characteristics of unsaturated soil deviate from those of typical soil mechanisms. The layers of soil on top of the groundwater table are examples of soil that is being formed normally by nature [3, 4], while those in backfills and layered soil barrier systems are created artificially.

Since current geotechnical engineering operations mainly employ the usage of unsaturated soil over saturated soil, experimental studies on the parameters of unsaturated soil can reap many benefits. In unsaturated soil, the pore-water pressure (u_w) is lower than the pore-air pressure (u_a);

this accounts for its positive matric suction ($u_a - u_w$) [1, 5, 6]. The relative humidity of the pore-water vapour found in soil is defined by the matric and osmotic suction which makes up the whole suction structure [7]. Since the changes in osmotic suction are minuscule in relation to deviations in matric suction, the full suction may consider matric suction as the sole value for ease of computation; the reverse is also possible [1, 8, 9].

Numerous residual and colluvial soils are gap-graded and demonstrate bimodal grain size distribution (GSD) [10–14]. Mercer et al. [15] recorded that gap-graded soil is mainly correlated with dual porosity structure. Dual porosity soil (soil exhibiting bimodal soil-water characteristic curve or SWCC) comprises substantially large amounts of coarse soil particles and great amounts of small soil particles. This makes up the large pores and small pores, respectively [16].

The rationale behind the formation of the two summits within the pore-size distribution function was being researched upon by [17]. They inferred that the occurrence

of two different porous systems within the capillary domain created the bimodal pattern of the SWCC. The porous systems are matrix (intra-aggregate, textural, micro) pores inside soil aggregates and structural (interaggregate, macro) pores between the aggregates.

The soil-water hydrostatics in the matrix domain is directly related to the arrangement of the soil skeleton. The shape, size, and stability of the aggregates are also factors affecting the linkage between structural pores. The air entry value of the matrix pores is the separating screen between matrix and structural pores. It also corresponds to the amount of residual water in the structural pores [18]. Typical structure and pore size distribution of a dual porosity soil (soil with bimodal SWCC) are presented in Figure 1. Feuerharmel et al. [19] recorded that SWCCs of most colluvium soils exhibit clear bimodal properties that correspond to the bimodal features of GSD. Soil with bimodal characteristics of SWCC has two air entry values, two inflection points, and two standard deviations due to the presence of large pores and small pores within the soil matrix. Figure 1 presents the typical shape of dual porosity soil (soil with bimodal SWCC) with its variables.

The matric suction has a function linked to the water content present in soil. Volumetric water content, gravimetric water content, or level of saturation can all be associated with the water content here [1]. As such, the water content can be drawn against matric suction values to obtain the SWCC. The SWCC can be used as a forecast for the absorption rate of unsaturated soils [20].

Typical models of SWCCs consist mainly of the unimodal form (one curve) or bimodal form (two subcurves). Correlations can also be drawn between the outlying form of the grain size distribution (GSD) curve and the SWCC. Historical researches pointed towards the indication that bimodal GSD soils are more probable to have bimodal pore size distributions [21], where the dual porosity is created by macropores and micropores. Saturated water content and dry density can act as indicators for the type of bimodal and unimodal characteristics that are demonstrated in the SWCC for soils with bimodal GSD [16, 22, 23]. The fine grains are unable to completely patch the empty voids between the larger grains; therefore, a bimodal SWCC would give rise to a bimodal pore size distribution [13].

The confining pressure applied on soil is one of the factors affecting its SWCC [24, 25]. Ng and Pang [25] determined that the greater the net confining pressure applied on the soil, the greater the air entry value, and the slope of the SWCC is more gradual. Lee et al. [24] illustrate the test results showing that there is an inverse relationship between

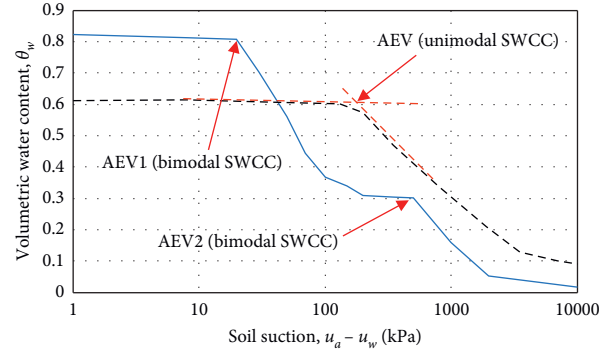


FIGURE 1: Soil with bimodal SWCC.

applied net confining pressure, at any given matric suction, and the saturated volumetric water content. However, it has a direct relationship with AEV in the soil.

Residual soils (dual-porosity soil) with two subcurves of SWCC can be found in many places in Singapore [26]. The soils located in different depths have different confining pressures. Residual soils are commonly located in the unsaturated zones due to the deep groundwater tables. Tropical regions like Singapore experience many rainfalls throughout the year [4]. The water infiltration into the soil layer results in pore-water pressure variations during rainy period. Hence, it will affect the behavior of dual porosity soil [27]. Other studies have also been conducted to investigate the SWCC of cohesive and noncohesive soils by Fattah et al. [28], Abd et al. [29], Fattah et al., [30], Abd et al. [31], and Fattah et al. [32].

Past studies only focused on the investigation of the variations of SWCC for unimodal soil due to different confining pressure. There are no studies on the effect of confining pressure on SWCC with bimodal characteristics or dual porosity soil. Examining the various possible outcomes on the SWCC of dual porosity soil with different confining pressure is the primary aim of this study. The scope of this study involves measurements of drying and wetting SWCC using Tempe cells, pressure plates, and an advanced triaxial apparatus. In addition, mathematical equations were developed to understand the effect of confining pressure on SWCC of dual porosity soils.

2. Applicable Theories

The GSD equation for the best fitting bimodal GSD used in this study was developed by [16] as shown in

$$P = \left[1 - \left(\frac{\ln(1 + (d_r/d))}{\ln(1 + (d_r/d_{\min}))} \right) \right] \left[W_1 \left(\operatorname{erfc} \frac{\ln(((d_{\max 1} - d_{m1})/(d_{\max 1} - d)))}{s_{d1}} \right) + W_2 \left((\beta_1) + (\beta_2) \operatorname{erfc} \frac{\ln(((d_{\max 2} - d_{m2})/(d_{\max 2} - d)))}{s_{d2}} \right) \right]. \quad (1)$$

Here, we have the following:

P = cumulative grain-size distribution of soil

$\beta_1 = 1$ when $d \leq d_{\max 2}$; $\beta_1 = 0$ when $d > d_{\max 2}$

$\beta_2 = 0$ when $d \leq d_{\max 2}$; $\beta_2 = 1$ when $d > d_{\max 2}$

d = diameter of soil particle (mm)

d_r = parameter representing the maximum particle size of fine particles

d_m = parameter representing the geometric mean of soil particle diameter (mm)

d_{\min} = parameter representing the minimum particle size that can be measured using hydrometer analysis (typical value = 0.0001 mm)

d_{\max} = parameter representing the maximum diameter of soil particle (mm)

s_d = parameter representing the geometric standard deviation of GSD curve

W = parameter representing the proportion of soil particle within coarse- or fine-grained particles

$$s_d = (\%d_{0.001}) \exp \sqrt{\frac{\sum_{i=1}^n (\ln(d_i/d_m))}{n}}, \quad (2)$$

d_m = geometric mean of soil particle

$\%d_{0.001}$ = percentage of soil particle with diameter smaller than 0.001 mm

$$d_m = \sqrt[n]{d_1 d_2 \dots d_n}. \quad (3)$$

Subscripts 1 and 2 represent subcurves 1 and 2, respectively.

For SWCC curves that display bimodal properties, equation (4) proposed by [16] was used:

$$\theta_w = \left(1 - \frac{\ln(1 + (\psi/\psi_r))}{\ln(1 + (1000000/\psi_r))} \right) \cdot \left[\theta_r + (\theta_{s1} - \theta_{s2}) \left(1 - \operatorname{erfc} \frac{\ln(((\psi_{a1} - \psi)/(\psi_{a1} - \psi_{m1})))}{s_1} \right) + (\theta_{s2} - \theta_r) \left(1 - \operatorname{erfc} \frac{\ln(((\psi_{a2} - \psi)/(\psi_{a2} - \psi_{m2})))}{s_2} \right) \right], \quad (4)$$

where we have the following:

θ_w = determined volumetric water content

θ_s = volumetric water content in saturated condition

θ_r = volumetric water content in residual condition

$$\psi = (u_a - u_w) \text{ (kPa)}, \quad (5)$$

$\psi_r = (u_a - u_w)$ at residual condition (kPa)

$\psi_m = (u_a - u_w)$ associated with dominant pore size (kPa)

ψ_a = air-entry value of soil (kPa)

s = SWCC geometric standard deviation

erfc = the complimentary error function

Subscripts 1 and 2 represent subcurves 1 and 2, respectively

3. Research Program

Laboratory tests were conducted on compacted soils in order to investigate the influence of confining pressure on bimodal SWCC. The compacted soils were produced by mixing coarse kaolin and Ottawa sand. The compacted soils were used in the research to avoid the heterogeneity of the soils for better analyses. ASTM graded sand, Ottawa sand, which is furnished by U.S. Silica Company, was selected to be mixed with the coarse kaolin which is produced by Kaolin Malaysia SDN BHD (Malaysia) to produce the sand-kaolin mixture. The index properties of the soil mixture of 50% kaolin and 50% Ottawa sand was obtained from the Atterberg limits

test, grain size distribution test, hydrometer test, and specific gravity test. Index properties tests were carried out following the ASTM standards [33–37].

Following the steps recorded in [38], static compaction was performed. Even mixing of the soil was done manually. The water content started off at 12.2%, which correlates with the 95% maximum dry density at the dry optimum conditions of the compaction curve. Three separate soil samples with the same weight were obtained from the initial sample and put inside three circular moulds 50 mm wide. Uniform compaction using a static compaction machine then occurs to create folds of 10 mm with constant loading rate at 1 mm per minute. Lastly, physical data (i.e., weight and dimensions) for the 30 mm × 50 mm specimen were determined after it was extruded. The experimental works to obtain drying and wetting SWCC were conducted using Tempe cell, pressure plate [39], and modified triaxial cell. The relevant procedures and equipments for each tests are explained in Subsections 3.1–3.3.

3.1. SWCC Testing Using Tempe Cell. Tempe cell is mainly utilized at low pressures of one to hundred kilopascals, whereas the pressure plate was used at higher pressures of hundred to five hundred kilopascals [40]. Daily recording of the mass of the specimen was then to be taken. Following the formation of the soil specimen, with equal proportions of kaolin and sand, it was then tailored so that it goes precisely into the brass cylinder. Application of deoxygenated purified water by operating the vacuum desiccator onto the porous ceramic plate will make it completely saturated. The brass

cylinder is then rested onto the plate. The volume of the cylindrical specimen can be obtained using the data of its height and diameter. Figure 2 depicts the setup of the Tempe cell. The main part of the Tempe cell and pressure plate is the porous ceramic plate.

The procedures of SWCC testing were carried out following the study in [42]. Prior to linking up the Tempe cell to the pressure outlet of the manifold, saturation of the soil specimen was performed. The saturation process was ceased when the water content of the soil specimen reached its saturated value. After the saturation stage, the weight of the saturated specimen and the Tempe cell was recorded. The air pressure system was connected from the top of the Tempe cell. Air pressure was then applied to the specified value to create respective matric suction in the soil specimen. Air would not flow through the porous ceramic plate when higher air pressure was introduced into the cell, as long as the air pressure did not exceed the air-entry value of the ceramic plate and the ceramic plate was kept saturated. For this reason, the bottom of the Tempe cell was connected to a container filled with water to maintain the degree of saturation of the ceramic plate. Weighing of the specimen at regular intervals was necessary to obtain sufficient data for the plot of the water volume change in the specimen at various matric suctions. The ceramic disk and water compartment were flushed every time after the readings were taken to ensure that the ceramic disk and the water compartment are in saturated condition.

Monitor and increase the air pressure inside the cell to the required amount using pressure gauges. By increasing the pore-air pressure (u_a), it meant that the matric suction ($u_a - u_w$) would increase because the pore-water pressure (u_w) remained at zero throughout the SWCC test. When measurements of the mass of the specimen need to be taken at the scheduled time intervals, the Tempe cell will be unplugged from the pressure outlet. After no further increase in mass is observed, the air pressure was turned up and this will cause the matric suction ($u_a - u_w$) in the Tempe cell to be increased. Rerun these steps until the final matric suction ($u_a - u_w$) is obtained. The drying SWCC measurement followed the matric suction incremental steps of 0.5, 1, 3, 5, 10, 20, 30, 40, 60, and 80 kPa. Then, the specimen was moved into pressure plate. Once the drying process in pressure plate is completed, the wetting process was started. The wetting process was conducted by reducing the matric suction within the soil specimen. The wetting SWCC measurement at Tempe cell followed the matric suction decremental steps of 50, 20, 10, 5, and 1 kPa.

3.2. SWCC Testing Using Pressure Plate. Operations at elevated pressure scale higher ($u_a - u_w$), requiring a pressure plate to be employed. Pressure plate consists of a pressure chamber that contains a saturated ceramic plate. The pressure plate was connected to a burette for measurement of water volume change and maintenance of degree of saturation of the ceramic plate. There must be a good contact between the soil specimen and the ceramic plate to ensure the water flow between the specimen and the plate is

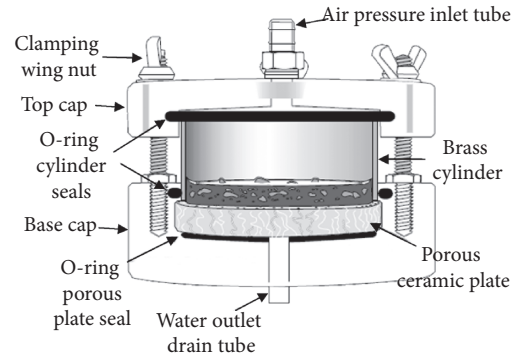


FIGURE 2: Schematic diagram of Tempe cell sample [41].

continuous. The highest air pressure applied on the pressure plates in this study is 400 kPa. Figure 3 illustrates the setup of a pressure plate which comprises a chamber with a pressure plate cell and a burette being held vertically upright using a stand. Throughout this experiment, the soil specimen was taken out of the pressure plate at designated time intervals to take measurements of its mass. After no significant change in mass was being observed, the air pressure was raised to increase the matric suction ($u_a - u_w$) in the pressure plate. These steps were repeated until the final matric suction ($u_a - u_w$).

The drying SWCC measurement at pressure plate followed the matric suction incremental steps of 100, 200, and 400 kPa. Once the drying process in pressure plate is completed, the wetting process was started. The wetting SWCC measurement at pressure plate followed the matric suction decremental steps of 200 and 100 kPa.

3.3. SWCC Testing Using Modified Triaxial Cell. Modified triaxial cell was utilized to perform SWCC tests with the application of confining pressures. A modified triaxial apparatus, as described by [1], was used for conducting the SWCC tests. A 5-bar high air-entry ceramic disk with a thickness of 6.35 mm and a diameter of 50 mm was sealed on the pedestal by applying slow settling epoxy glue along its circumference. The specimen was placed directly on the saturated ceramic disk while filter paper, coarse corundum stone, and top cap were placed on top of the specimen. Rubber membrane was put on the specimen and secured with O-rings at the top cap as well as the pedestal. All specimens were saturated at the beginning of the test to have a uniform initial condition and to reduce the matric suction to a low value. Saturation was performed by applying cell pressure, σ_3 , and back pressure, u_w , from digital pressure and volume controller (DPVC). A net confining pressure of 10 kPa was maintained to prevent significant swelling of the specimen until the pore-water pressure parameter, B , was larger than 0.95 as suggested by [43].

Isotropic consolidation of the specimen was applied directly after saturation. Consolidation ceases only after the equilibrium phase in the pore-water volume is achieved. Once consolidation was completed, drying process of the

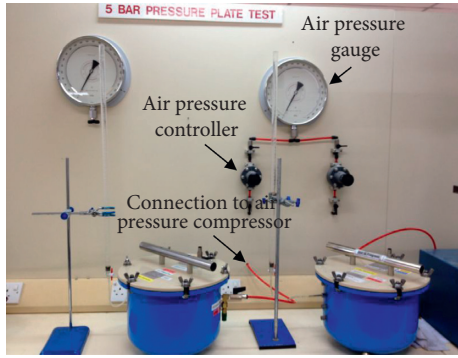


FIGURE 3: Pressure plate setup.

SWCC was conducted by applying the designated matric suction using the axis translation technique [44]. Pore-water and cell pressures and volume changes were applied and controlled by DPVCs. Drying process of SWCC was achieved by following the designated incremental steps of matric suction while wetting process of SWCC was achieved by following the designated decremental steps of matric suction. After the matric suction and water volume change reached equilibrium, the matric suction was increased to next step by decreasing the pore-water pressure while maintaining constant confining and pore-air pressures. After the specimen reached the maximum matric suction 440 kPa in this research, wetting stage of the specimen was started by increasing the pore-water pressure while maintaining constant confining and pore-air pressures. Before incrementing or decrementing matric suction, the water compartment was flushed to remove diffused air from the water compartment.

4. Presentations and Results

The results of index property tests are shown in Table 1. The grain size distribution curve of the soil mixture is presented in Figure 4.

Figure 5 illustrates the compaction curve derived, which is established by the dry density and water content determined for the respective soil samples. It also indicates the 95% maximum dry density and the maximum dry density. Figure 5 shows that the optimum dry density is 1.84 Mg/m³ at 14.2% water content. The 95% maximum dry density at the dry optimum condition is 1.75 Mg/m³ at 12.20% water content. Figure 6 illustrates the SWCC obtained from Tempe cell tests.

The SWCC data from laboratory tests were best fitted using (4). Then, the fitting parameter was compared with the variables of SWCC (i.e., AEV1, AEV2, inflection point 1, and inflection point 2) that were manually determined from the SWCC curve graph. Hence, the fitting parameters are close to the variables of SWCC. Therefore, the fitting parameters from (4) were used to determine SWCC variables. The fitting parameters of SWCC in the Tempe cell tests are collated in Table 2. The air entry value 1 is 10 kPa, the air entry value 2 is 40 kPa, the inflection point 1 is 15 kPa, the inflection point 2 is 105.6 kPa, the standard of deviation 1 is 0.5, and the

TABLE 1: Basic properties of 50% Ottawa sand and 50% kaolin.

Index properties	50% sand-50% kaolin
Specific gravity, G _s	2.59
Plastic limit, PL (%)	27
Liquid limit, LL (%)	47
Plasticity index, PI (%)	20
Void ratio, e	0.48
Dry density, ρ _d (Mg/m ³)	1.65
Water content, w (%)	11
Sand (%)	50.0
Silt (%)	43.7
Clay (%)	6.3
Soil classification according to USCS	SM

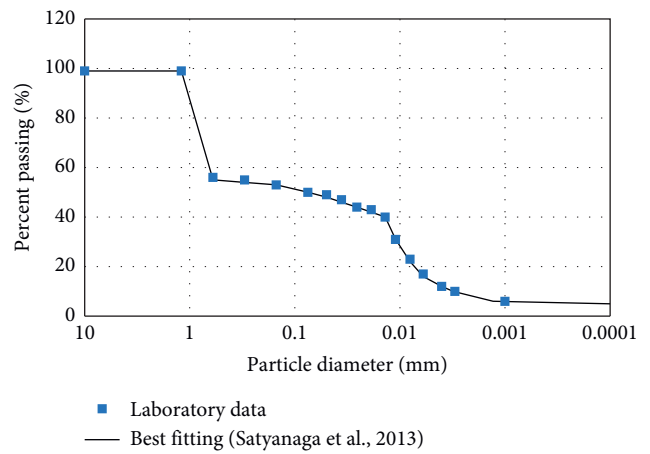


FIGURE 4: Grain size distribution of the investigated soil.

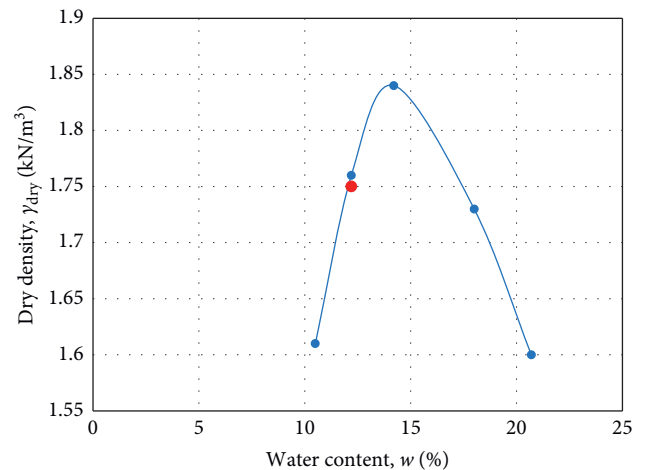


FIGURE 5: Compaction curve.

standard of deviation 2 is 1.202 for the drying curve. The inflection point is 5 kPa for the wetting curve.

Figure 7 shows the SWCC from Triaxial Test with 25 kPa of net confining pressure. The determination of SWCC variables follow the same procedures as performed for SWCC data in Figure 6. The fitting parameters of SWCC from triaxial cell tests with 25 kPa net confining pressure are

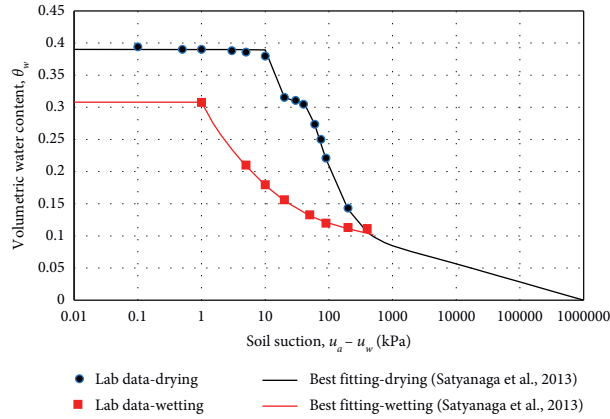


FIGURE 6: SWCC of the investigated soil from Tempe cell test.

TABLE 2: Fitting parameters of SWCC data.

Confining pressure (kPa)	0	25	50	75
AEV 1 (kPa)	10	12	20	30
AEV 2 (kPa)	40	60	90	200
Inflection point 1 (drying) (kPa)	15	20	35	50
Inflection point 2 (drying) (kPa)	106	200	300	650
Standard deviation 1 (drying)	0.5	0.6	0.65	0.75
Standard deviation 2 (drying)	1.2	1.35	1.35	1.5
Water-entry value (kPa)	500	700	1000	2000
Mode of test	Tempe cell + pressure plate	Modified triaxial	Modified triaxial	Modified triaxial

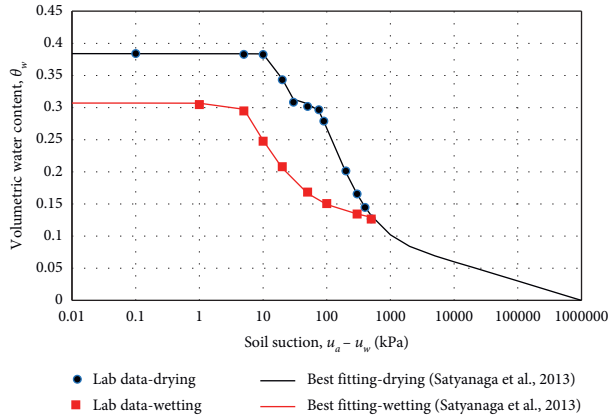


FIGURE 7: SWCC using Triaxial Test with 25 kPa confining pressure.

summarized in Table 2. The air entry value 1 is 12 kPa, the air entry value 2 is 60 kPa, the inflection point 1 is 20 kPa, the inflection point 2 is 200 kPa, the standard of deviation 1 is 0.6, and the standard of deviation 2 is 1.35 for the drying curve. The inflection point is 15 kPa for the wetting curve.

Figure 8 shows the SWCC for Triaxial Test with 50 kPa confining pressure. The determination of SWCC variables follows the same procedures as performed for SWCC data in Figure 6. The fitting parameters of SWCC from triaxial cell tests with 50 kPa net confining pressure are summarized in Table 2. The air entry value 1 is 20 kPa, the air entry value 2 is

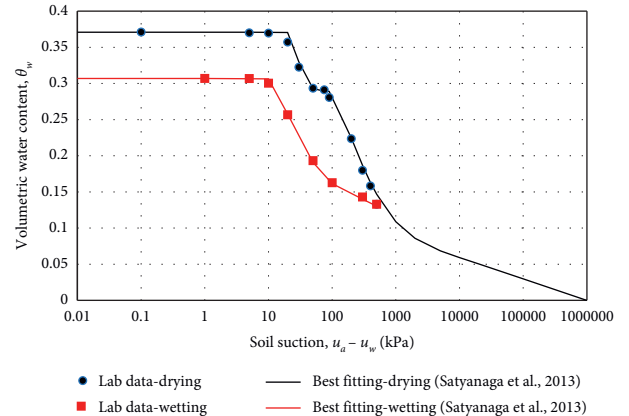


FIGURE 8: SWCC test using triaxial test with 50 kPa confining pressure.

90 kPa, the inflection point 1 is 35 kPa, the inflection point 2 is 300 kPa, the standard of deviation 1 is 0.65, and the standard of deviation 2 is 1.35 for the drying curve. The inflection point is 30 kPa for the wetting curve.

Figure 9 shows the SWCC for Triaxial Test with 75 kPa net confining pressure. The determination of SWCC variables follows the same procedures as performed for SWCC data in Figure 6. The fitting parameters of SWCC from triaxial cell tests with 75 kPa net confining pressure are summarized in Table 2. The air entry value 1 is 30 kPa, the air entry value 2 is 200 kPa, the inflection point 1 is 50 kPa, the

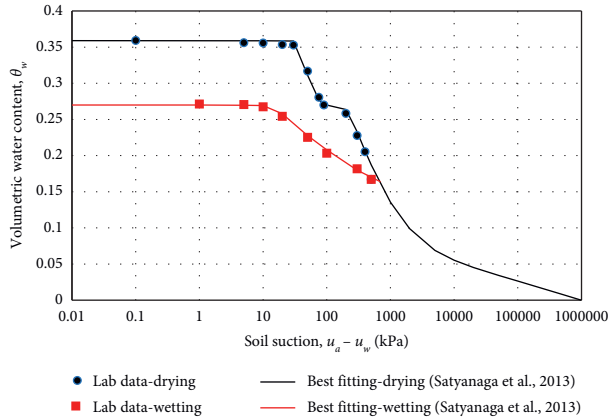


FIGURE 9: SWCC test using Triaxial Test with 75 kPa confining pressure.

inflection point 2 is 650 kPa, the standard of deviation 1 is 0.75, and the standard of deviation 2 is 1.5 for the drying curve. The inflection point is 75 kPa for the wetting curve.

5. Discussion

Based on the SWCC data presented in Section 5, the Air Entry Value increases with the increase of the net confining pressure as illustrated in Figures 10 and 11. SWCC tests with 0 kPa net confining pressure generated the lowest Air Entry Value, whereas SWCC tests with 75 kPa net confining pressure produced the highest Air Entry Value. This could happen since the higher the net confining pressure, the higher the density of the soil and hence the pores become smaller and it makes water more difficult to flow out of the pores. Figure 10 shows that $AEV1 = 0.272$ (confining pressure) + 7.8. Figure 10 shows that $AEV2 = 2.04$ (confining pressure) + 21.

Based on the SWCC data, the inflection point within subcurve 1 and subcurve 2 of the SWCC increases with the increase in the net confining pressure as illustrated in Figures 12 and 13. SWCC tests with 0 kPa net confining pressure produced the lowest inflection point, whereas SWCC tests with 75 kPa net confining pressure generated the highest inflection point. This might happen since the higher net confining pressure results in slower water flows out from the pores of the soil for suctions beyond Air Entry Values of the soil. Figure 12 indicates that inflection point 1 = 0.48 (confining pressure) + 12. Figure 13 shows that inflection point 2 = 6.93 (confining pressure) + 54.

Based on the SWCC data, the standard deviation of SWCC increases with the increase in the net confining pressure as illustrated in Figures 14 and 15. SWCC tests with 0 kPa net confining pressure generated the lowest standard deviation value, whereas SWCC tests with 75 kPa net confining pressure produced the highest standard deviation of SWCC. This might happen since the higher the standard deviation of SWCC, the gentler the slope of SWCC graphs and hence water flows slower from the pores of the soil for suctions beyond the air entry values. Figure 14 indicates that standard deviation 1 = 0.0032 (confining pressure) + 0.505.

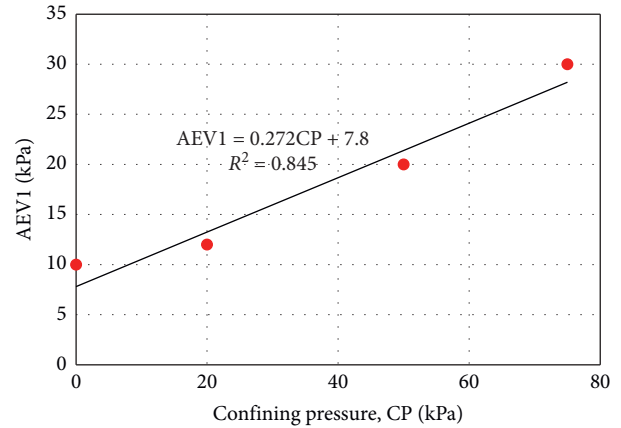


FIGURE 10: A graph of air entry value 1 with confining pressure.

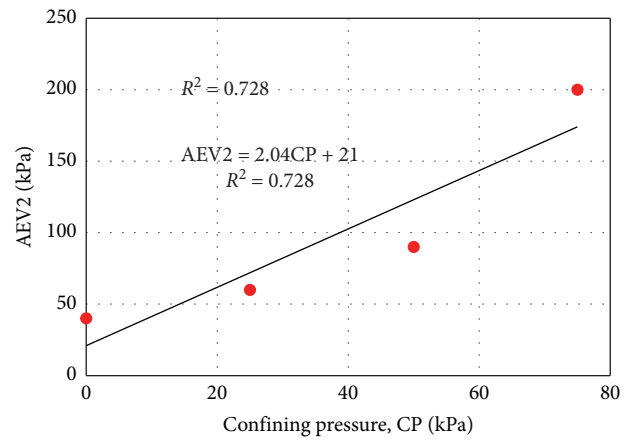


FIGURE 11: A graph of air entry value 2 with confining pressure.

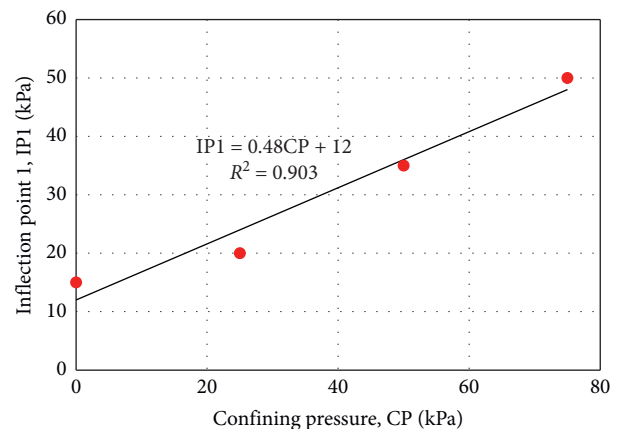


FIGURE 12: A graph of inflection point 1 with confining pressure.

Figure 15 shows that standard deviation 2 = 0.0036 (confining pressure) + 1.216.

Based on the observation of all SWCC, the drying curve exhibits bimodal characteristics, but the wetting curve exhibits unimodal characteristics. The difference in the drying curve and wetting curve was because of the rearrangement of

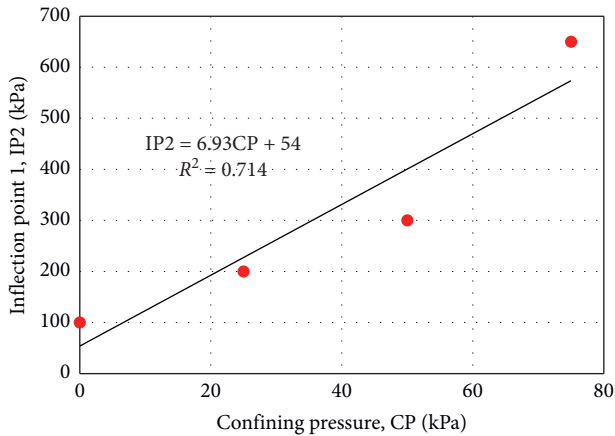


FIGURE 13: A graph of inflection point 2 with confining pressure.

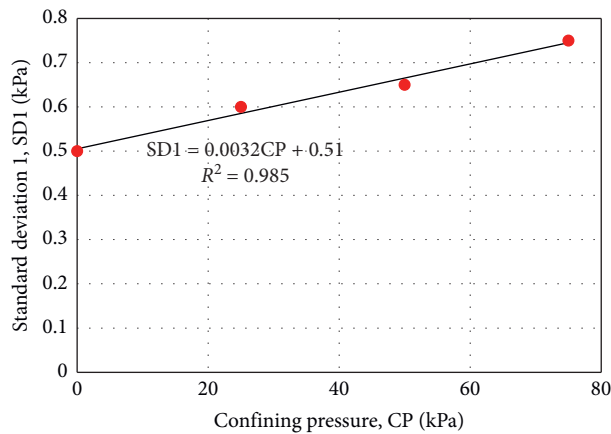


FIGURE 14: A graph of standard deviation 1 against confining pressure.

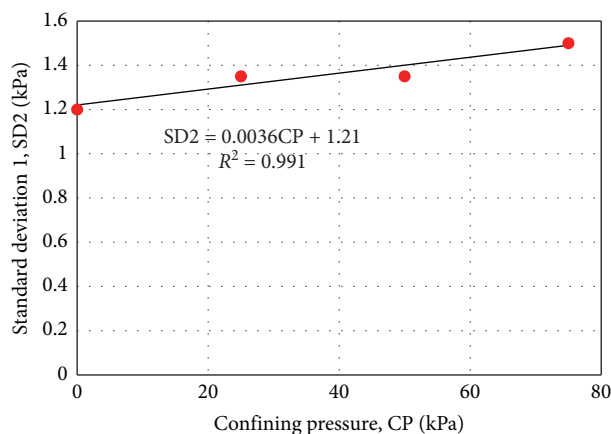


FIGURE 15: A graph of standard deviation 2 with confining pressure.

soil particles and the entrapped air. The rearrangement of the soil particles might happen since the soil experienced a volume change (shrink) during the drying process. Hence, there was no more entrapped pores during wetting process and SWCC became unimodal. The drying process also

resulted in the entrapped air within the pores of the soil. Therefore, during the wetting phase, the soil specimen is unable to absorb back the same amount of water.

Based on the SWCC data, the water-entry value increases with the increase in the net confining pressure, as presented in Table 2. Wetting SWCC tests with 0 kPa net confining pressure generated the lowest water-entry value, whereas wetting SWCC tests with 75 kPa net confining pressure produced the highest water-entry value. This could happen since the higher the net confining pressure, the higher the density of soil. As a result, the soil pore is smaller and the water is more difficult to flow into the soil pore.

6. Conclusions

In conclusion, for the dual porosity soil, it exhibits a bimodal SWCC for the drying curve and it exhibits a unimodal SWCC for the wetting curve. The rearrangement of the soil particles and entrapped air brought about the difference between the drying and wetting curves.

As the net confining pressure increases, the air entry value increases, which is due to the increase in the density of the soil. When the net confining pressure rises, the inflection points on the drying curve increase, which shows that there is a decrease in the rate of water flowing out after the air entry values. As the net confining pressure increases, the standard deviation increases.

For the wetting curve of the SWCC, as the net confining pressure increases, the water-entry value increases. As the net confining pressure increases, the soil pore is smaller and the water is more difficult to flow into the soil pore.

This study is limited to sandy soil with no significant volume change. Further studies must be conducted to investigate the effect of confining pressure on fine-grained soil with high volume change.

Data Availability

The experimental data used to support the findings of this study are included within the article.

Conflicts of Interest

The authors declare no conflicts of interest.

Acknowledgments

The authors thank Universitas Bina Darma for providing the funding and preparing the data so that the paper could be completed.

References

- [1] D. G. Fredlund and H. Rahardjo, *Soil Mechanics for Unsaturated Soils*, John Wiley & Sons, Inc., New York, NY, USA, 1993.
- [2] S. G. Goh, H. Rahardjo, and E. C. Leong, "Shear strength equations for unsaturated soil under drying and wetting," *ASCE Journal of Geotechnical and Geoenvironmental Engineering*, vol. 136, no. 4, pp. 594–606, 2010.

- [3] H. Rahardjo, A. S. Nio, E. C. Leong, and J.-Y. Wang, "Comprehensive instrumentation for real time monitoring of flux boundary conditions in slope," *Procedia Earth and Planetary Science*, vol. 9, pp. 23–43, 2014.
- [4] H. Rahardjo, A. Satyanaga, E. C. Leong, Y. S. Ng, M. D. Foo, and C. L. Wang, "Slope failures in Singapore due to rainfall," in *Proceedings of 10th Australia New Zealand Conference on Geomechanics "Common Ground"*, pp. 704–709, Brisbane, Australia, October 2007.
- [5] H. Rahardjo, Y. Kim, and A. Satyanaga, "Role of unsaturated soil mechanics in geotechnical engineering," *International Journal of Geo-Engineering*, vol. 10, no. 1, 2019.
- [6] A. Satyanaga and H. Rahardjo, "Stability of unsaturated soil slopes covered with melastoma malabathricum in Singapore," *Geotechnical Engineering*, vol. 7, no. 6, pp. 393–403, 2020.
- [7] G. D. Aitchison, *Moisture Equilibria and Moisture Changes in Soils beneath Covered Areas Statement of the Review Panel, Engineering Concepts of Moisture Equilibria and Moisture Changes in Soils*, Butterworths, London, UK, 1965.
- [8] D. G. Fredlund, A. Xing, and S. Huang, "Predicting the permeability function for unsaturated soils using the soil-water characteristic curve," *Canadian Geotechnical Journal*, vol. 31, no. 4, pp. 533–546, 1994.
- [9] A. Satyanaga and H. Rahardjo, "Role of unsaturated soil properties in the development of slope susceptibility map," *Proceedings of the Institution of Civil Engineers - Geotechnical Engineering*, vol. 16, pp. 1–44, 2020.
- [10] A. Jotisankasa, H. Vathananukij, and M. R. Coop, "Soil-water retention curves of some silty soils and their relations to fabrics," in *Proceedings of the 4th Asia Pacific Conference on Unsaturated Soils*, pp. 263–268, Newcastle, Australia, November 2009.
- [11] H. Rahardjo, A. Satyanaga, G. A. R. D'Amore, and E.-C. Leong, "Soil-water characteristic curves of gap-graded soils," *Engineering Geology*, vol. 125, pp. 102–107, 2012.
- [12] A. Satyanaga and H. Rahardjo, "Unsaturated shear strength of soil with bimodal soil-water characteristic curve," *Géotechnique*, vol. 69, no. 9, pp. 828–832, 2019.
- [13] L. Zhang and Q. Chen, "Predicting bimodal soil-water characteristic curves," *Journal of Geotechnical and Geoenvironmental Engineering*, vol. 131, no. 5, pp. 666–670, 2005.
- [14] Q. Zhai, H. Rahardjo, A. Satyanaga, and Priono, "Effect of bimodal soil-water characteristic curve on the estimation of permeability function," *Engineering Geology*, vol. 230, pp. 142–151, 2017.
- [15] K. Mercer, H. Rahardjo, and A. Satyanaga, "Unsaturated soils guidelines – volume 1," in *Soil-Water Characteristic Curves for Materials Classified According to the Unified Soil Classification System*, p. 154, Australian Center for Geomechanics, University of Western Australia, Crawley, Western Australia, 2019.
- [16] A. Satyanaga, H. Rahardjo, E.-C. Leong, and J.-Y. Wang, "Water characteristic curve of soil with bimodal grain-size distribution," *Computers and Geotechnics*, vol. 48, pp. 51–61, 2013.
- [17] M. Kutilek and D. R. Nielsen, *Soil Hydrology*, Catena Verlag, Cremlingen Destedt, Cremlingen, Germany, 1994.
- [18] M. Kutilek, "Soil hydraulic properties as related to soil structure," *Soil and Tillage Research*, vol. 79, no. 2, pp. 175–184, 2004.
- [19] C. Feuerharmel, W. Y. Y. Gehling, and A. V. D. Bica, "The use of filter-paper and suction-plate methods for determining the soil-water characteristic curve of undisturbed colluvium soils," *Geotechnical Testing Journal*, vol. 29, no. 5, pp. 1–7, 2006.
- [20] D. G. Fredlund and A. Xing, "Equations for the soil-water characteristic curve," *Canadian Geotechnical Journal*, vol. 31, no. 4, pp. 521–532, 1994.
- [21] W. Durner, "Hydraulic conductivity estimation for soils with heterogeneous pore structure," *Water Resources Research*, vol. 30, no. 2, pp. 211–223, 1994.
- [22] Q. Zhai, H. Rahardjo, A. Satyanaga, G. Dai, and Y. Zhuang, "Framework to estimate the soil-water characteristic curve for soils with different void ratios," *Bulletin of Engineering Geology and the Environment*, vol. 79, no. 8, pp. 4399–4409, 2020.
- [23] Q. Zhai, H. Rahardjo, and A. Satyanaga, "A pore-size distribution function based method for estimation of hydraulic properties of sandy soils," *Engineering Geology*, vol. 246, pp. 288–292, 2018.
- [24] I.-M. Lee, S.-G. Sung, and G.-C. Cho, "Effect of stress state on the unsaturated shear strength of a weathered granite," *Canadian Geotechnical Journal*, vol. 42, no. 2, pp. 624–631, 2005.
- [25] C. W. W. Ng and Y. W. Pang, "Influence of stress state on soil-water characteristics and slope stability," *Journal of Geotechnical and Geoenvironmental Engineering*, vol. 126, no. 2, pp. 157–166, 2000.
- [26] A. Satyanaga, H. Rahardjo, and C. J. Hua, "Numerical simulation of capillary barrier system under rainfall infiltration," *ISSMGE International Journal of Geoenvironmental Case Histories*, vol. 5, no. 1, pp. 43–54, 2019.
- [27] A. Satyanaga, H. Rahardjo, and Q. Zhai, "Estimation of unimodal water characteristic curve for gap-graded soil," *Soils and Foundations*, vol. 57, no. 5, pp. 789–801, 2017.
- [28] M. Y. Fattah, Q. G. Majeed, and H. H. Joni, "Comparison between methods of soil saturation on determination of the soil water characteristic curve of cohesive soils," *Arabian Journal of Geosciences*, vol. 14, no. 2, 2021.
- [29] I. A. Abd, H. Mekkiyah, and M. Y. Fattah, "The soil water characteristic curve for non-cohesive soils," *Solid State Technology*, vol. 63, no. 1, pp. 720–729, 2020.
- [30] M. Y. Fattah, A. A. H. Al-Obaidi, and M. K. Al-Dorriy, "Determination of the soil water characteristic curve for unsaturated gypseous soil from model tests," *Research Journal of Applied Sciences*, vol. 13, no. 19, pp. 544–551, 2018.
- [31] I. A. Abd, M. Y. Fattah, and H. Mekkiyah, "Relationship between the matric suction and the shear strength in unsaturated soil," *Case Studies in Construction Materials*, vol. 13, Article ID e00441, 2020.
- [32] M. Y. Fattah, A. Y. Yahya, M. T. Al-Hadidi, and B. A. Ahmed, "Effect of salt content on total and matric suction of unsaturated soils," *European Scientific Journal*, vol. 9, no. 9, pp. 228–245, 2013.
- [33] ASTM D422-63, "Standard test method for particle-size analysis of soils," 2002.
- [34] ASTM D854-02, "Standard test methods for specific gravity of soil solids by water pycnometer," 2002.
- [35] ASTM D4318-00, "Standard test methods for liquid limit, plastic limit, and plasticity index of soils," 2000.
- [36] ASTM D2487-00, "Standard practice for classification of soils for, engineering purposes, unified soil classification system," 2000.
- [37] ASTM D698-00, "Standard test methods for laboratory compaction characteristics of soil using standard effort," 2000.
- [38] B. H. Ong, "Shear strength and volume change of unsaturated soil," Master of Engineering Thesis, Nanyang Technological University, Singapore, 1999.

- [39] ASTM D6838-02, "Standard test methods for the soil-water characteristic curve for desorption using hanging column, pressure extractor, chilled mirror hygrometer, or centrifuge," 2008.
- [40] A. Satyanaga, H. Rahardjo, Z. H. Koh, and H. Mohamed, "Measurement of a soil-water characteristic curve and unsaturated permeability using the evaporation method and the chilled-mirror method," *Journal of Zhejiang University-SCIENCE A*, vol. 20, no. 5, pp. 368–374, 2019.
- [41] Soil Moisture Equipment Corp, Commercial Publications, Santa Barbara, CA, USA, 1985.
- [42] H. Rahardjo, A. Satyanaga, H. Mohamed, S. C. Yee Ip, and R. S. Shah, "Comparison of soil-water characteristic curves from conventional testing and combination of small-scale centrifuge and dew point methods," *Geotechnical and Geological Engineering*, vol. 37, no. 2, pp. 659–672, 2019.
- [43] K. H. Head, *Manual of Soil Laboratory*, pp. 925–945, Wiley, New York, NY, USA, 1986.
- [44] J. W. Hilf, "An investigation of pore-water pressure in compacted cohesive soils," Ph.D. dissertation, U.S. Department of the Interior, Bureau of Reclamation, Design and Construction Division, Denver, CO, USA, 1956.